Chemosphere 308 (2022) 136191

Contents lists available at ScienceDirect

Chemosphere

journal homepage: www.elsevier.com/locate/chemosphere

Novel composite of Zn/Ti-layered double hydroxide coupled with MXene for the efficient photocatalytic degradation of pharmaceuticals

Anna Grzegórska [a,**], Izabela Wysocka [a], Paweł Głuchowski [b], Jacek Ryl [c], Jakub Karczewski [c], Anna Zielińska-Jurek [a,*]

[a] Department of Process Engineering and Chemical Technology, Faculty of Chemistry, Gdańsk University of Technology, G. Narutowicza 11/12, Gdańsk, 80-233, Poland
[b] Institute of Low Temperature and Structural Research, Polish Academy of Sciences, Okólna 2, Wrocław, 50-422, Poland
[c] Institute of Nanotechnology and Materials Engineering, Faculty of Applied Physics and Mathematics, Gdańsk University of Technology, G. Narutowicza 11/12, Gdańsk, 80-233, Poland

HIGHLIGHTS

- Zn/Ti layered double hydroxide coupled with MXene was synthesized for the first time.
- Effective photodegradation of commonly detected pharmaceuticals in a model seawater.
- LDH/MXene containing 2.5 wt% of MXene revealed the highest photoactivity.
- The main oxidizing species responsible for ibuprofen degradation are OH.• and holes (h^+).
- Acetaminophen degradation by Zn/Ti LDH-Ti_3C_2 proceeded in the presence of .•O_2^-.

GRAPHICAL ABSTRACT

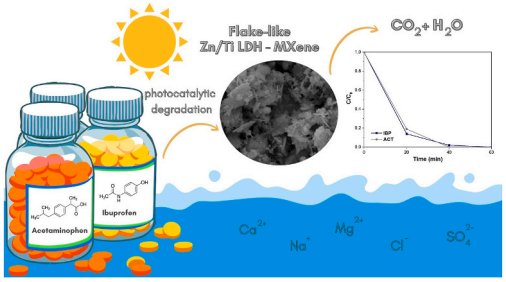

ARTICLE INFO

Handling editor: Sergi Garcia-Segura

Keywords:
Acetaminophen
Ibuprofen
MXene
Pharmaceuticals removal
Photocatalysis
Ti_3C_2
Zn/ti LDH

ABSTRACT

In the present study, a hybrid photocatalyst of Zn/Ti layered double hydroxide (LDH) coupled with MXene – Ti_3C_2 was synthesized for the first time and applied in photocatalytic degradation of acetaminophen and ibuprofen, two commonly present in the natural environment and prone to accumulate in the aquatic ecosystem pharmaceuticals. The effect of MXene content (0.5 wt%, 2.5 wt%, and 5 wt%) on the photocatalytic activity of LDH/MXene composite was investigated. The composite of LDH/MXene containing 2.5 wt% of MXene revealed the highest photocatalytic activity in the degradation of acetaminophen (100% within 40 min) and ibuprofen (99.7% within 60 min). Furthermore, an improvement in acetaminophen and ibuprofen mineralization was observed for the composite material. Meanwhile, the introduction of interfering ions (Na^+, Ca^{2+}, Mg^{2+}, Cl^-, SO_4^{2-}) in the model seawater did not affect the removal efficiency of both pharmaceuticals. The photocatalytic experiment performed in the four subsequent cycles, as well as FTIR, TEM, and XPS analyses after the photodegradation process confirmed the excellent stability and reusability of the prepared composite material. In order to evaluate the effect of various reactive oxidizing species (ROS) on the photocatalytic process, the trapping experiment was applied. It was noticed that •O_2^- had the main contribution in photocatalytic degradation of

* Corresponding author. Department of Process Engineering and Chemical Technology, Faculty of Chemistry, Gdańsk University of Technology, G. Narutowicza 11/12, Gdańsk, 80-233, Poland.,
** Corresponding author.
E-mail addresses: anna.grzegorska@pg.edu.pl (A. Grzegórska), annjurek@pg.edu.pl (A. Zielińska-Jurek).

https://doi.org/10.1016/j.chemosphere.2022.136191
Received 17 June 2022; Received in revised form 8 August 2022; Accepted 21 August 2022
Available online 26 August 2022

acetaminophen, while •OH and h^+ mainly affected the degradation of ibuprofen. Finally, based on the results of Mott Schottky analysis, bandgap calculation, and ROS trapping experiment, the possible mechanism for pharmaceuticals degradation was proposed. This research illustrates the feasibility and novelty of the treatment of pharmaceuticals by LDH/MXene composites, implying that MXene plays a significant role in the electron-hole separation and thus high photocatalytic activity.

1. Introduction

Water pollution is one of the present concerns for humans and the environment (Naz et al., 2021). The major impact is attributed to residues of pharmaceuticals, pesticides, nutrients, micro-plastics, and petroleum (Priya et al., 2022; Rasheed et al., 2020; Singh et al., 2021). Particularly, the important group includes pharmaceuticals, which concentration in water systems is continuously growing due to higher consumption and discharging as metabolites or unchanged forms into the environment (Desbiolles et al., 2018; Xiang et al., 2021). The contamination of water sources such as seawater or lake water brings the potential risk of chronic exposure of aquatic organisms, bioaccumulation, biomagnification, and thereby harmful effects on human health (Pemberthy M et al., 2020; Branchet et al., 2021).

Acetaminophen (ACT), commonly known as paracetamol, is an analgesic and antipyretic compound, while ibuprofen (IBP) belongs to the group of non-steroidal anti-inflammatory drugs (Dey et al., 2018). These pharmaceuticals are common in the natural environment and prone to accumulate in the aquatic ecosystem (Żur et al., 2011). Moreover, they have been detected in surface waters, wastewaters, as well as drinking waters around the world (Sousa et al., 2018). In Latin America, acetaminophen concentration was in the range of 0.016–46.6 μg/dm^3 in wastewaters and from 3 to 25,2 ng/dm^3 in surface waters. Meanwhile, ibuprofen concentration ranges from 220 to 13,000 ng/dm^3 in wastewaters and from 2 to 37,000 ng/dm^3 in surface waters (Peña-Guzmán et al., 2019). This shows that the commonly used wastewater treatment processes are ineffective in degrading some pharmaceutical compounds. Depending on the concentration and exposure time, these pollutants may be toxic to bacteria, algae, macrophytes, and fish (Phong Vo et al., 2019). Furthermore, depending on environmental conditions can transform into several more toxic and carcinogenic derivatives, for example, acetaminophen in 4-aminophenol or p-benzoquinone, while ibuprofen into 4-isobutylacetophenone (Liang et al., 2016; Ruggeri et al., 2013).

One of the promising methods for the degradation of emerging contaminants and treatment of active pharmaceutical ingredients is heterogeneous photocatalysis (Akpotu et al., 2019; Klementova et al., 2017). The application of inexpensive, highly available, chemically stable, and non-toxic photocatalysts classified it as a green remediation technology (Article et al., 2015; Xu et al., 2019).

The prospective materials in the field of photocatalysis are layered double hydroxides belonging to a class of two-dimensional semiconductors consisting of mixed metal hydroxide layers with anions or solvent molecules intercalated between them (Razzaq et al., 2020; Guo et al., 2010). However, the major drawbacks of LDH are low efficiency in the utilization of visible light and fast recombination of electron-hole pairs (Motlagh et al., 2020). Thus, the combination of LDH with other materials has been developed to overcome these limitations. For example, Zn/Ti-LDH were applied for methylene blue decomposition, rhodamine B and NO decomposition (Shao et al., 2011; Zhu et al., 2018), oxidation of benzyl alcohol (Zou et al., 2020) and photocatalytic toluene degradation in the gas phase (Liu et al., 2022). Zhu et al. (2017) proposed the combination of Zn/Ti LDH with C60 molecules. The synthesized material was applied for the photocatalytic decomposition of Orange II under simulated solar light. Furthermore, carbon-based materials are increasingly being used in photocatalytic processes (Tayyab et al., 2022; Liu et al., 2021a). The heterojunction of Zn/Ti LDH with g-C_3N_4 improved the photocatalytic efficiency of ceftriaxone sodium degradation and hydrogen generation under visible light (Sun et al., 2019).

Recently, MXene compounds with graphene-like morphology have become promising materials instead of platinum or palladium as noble-metal-free co-catalyst. These structures can inhibit the recombination of charge carriers, improve interfacial charge transfer, and increase photocatalytic activity. Previously, LDH/MXene composites were used for high-performance supercapacitors, adsorbents, sensors, electromagnetic wave absorbers, and catalysts in oxygen evolution reactions (OER) (Hao et al., 2019; Li et al., 2019a; Zhou et al., 2020). There are only a few studies on the application of LDH/MXene composites in photocatalysis. Chen et al. (2020) proposed the implementation of Co–Co LDH/$Ti_3C_2T_x$ for visible-light-driven photocatalytic CO_2 reduction. Wang et al. (2021a) applied a 3D marigold-like CoAl-LDH/Ti_3C_2 for the degradation of tetracycline hydrochloride, chloramphenicol, and terramycin. Meanwhile, Ma et al. (2022) used NiFe-LDH/MXene for photocatalytic removal of norfloxacin.

In this study, for the first time, Zn/Ti LDH-MXene composite was synthesized and used for photocatalytic degradation of two commonly detected pharmaceuticals - acetaminophen and ibuprofen under simulated solar light. The photocatalytic process of active pharmaceutical ingredients degradation was performed in model seawater to evaluate the effect of the multiple interfering ions on the removal efficiency. Furthermore, the physicochemical properties and optimal content of Ti_3C_2 in the hybrid photocatalyst were determined and the mechanism of photocatalytic degradation in the presence of reactive oxygen species was proposed.

2. Experimental

2.1. Materials

The MAX phase compound - Ti_3AlC_2 was provided by Luoyang Tongrun Info Technology Co. (China). The hydrofluoric acid (ACS reagent, 48%), $Zn(NO_3)_2{\cdot}6H_2O$ (reagent grade, 98%), $TiCl_4$ (ReagentPlus®, 99.9% trace metals basis), and urea (ReagentPlus®, ≥99.5%, pellets) were purchased from Sigma Aldrich. Acetaminophen (BioXtra, ≥99.0%) and Ibuprofen (≥98% (GC)) for the photocatalytic degradation process were provided by Sigma Aldrich. Scavengers: p-benzoquinone (reagent grade, ≥98%) and ammonium oxalate monohydrate (ACS reagent, ≥99%) were purchased from Sigma Aldrich, while isopropanol (99.7%, pure p. a.) and H_2O_2 (30%, pure p. a.) from Avantor Performance Materials Poland. The reagents were used as received with no further purification. Deionized water (DI) was used in all experiments.

2.2. The synthesis procedure of photocatalyst

2.2.1. Etching of Al from Ti_3AlC_2

First, the 10 g of MAX phase compound - Ti_3AlC_2 was added to 100 cm^3 of HF and mixed at room temperature. The material was rinsed with DI water and centrifuged until pH of 7. The powder was dried at 50 °C for 2 h under air conditions.

2.2.2. Synthesis of Zn/Ti LDH

In a typical procedure, 1.19 g of zinc nitrate hexahydrate was dissolved in 100 cm^3 DI water. Next, 0.22 cm^3 of $TiCl_4$ was added dropwise. The molar ratio of Zn to Ti was 2:1. Then 3.0 g of urea was added, and the mixture was magnetically stirred for 30 min. Subsequently, the

mixture was transferred to the 200 cm^3 Teflon-lined stainless steel autoclave. The reaction was performed at 130 °C for 48 h. Finally, the obtained material was centrifuged and washed with DI water until neutral pH. The powder was dried at 50 °C for 2 h under air condition.

2.2.3. Synthesis of Zn/Ti LDH-MXene

$Ti_3C_2T_x$ (0.5, 2.5, and 5 wt%) was dispersed in 100 cm^3 DI water and sonicated for 30 min. Then 1.19 g of zinc nitrate hexahydrate was dissolved in the above mixture. Next, 0.22 cm^3 of $TiCl_4$ was added dropwise. Then 3.0 g of urea was added, and the mixture was magnetically stirred for 30 min. Subsequently, the mixture was transferred to the 200 cm^3 Teflon-lined stainless steel autoclave. The reaction was performed at 130 °C for 48 h. Finally, the obtained material was repeatedly centrifuged and washed with DI water until neutral pH. The powder was dried at 50 °C for 2 h under air conditions. To evaluate the effect of synthesis conditions on the physicochemical properties of $Ti_3C_2T_x$, pure $Ti_3C_2T_x$ was solvothermal treated in the same conditions without precursors of Zn/Ti LDH. The scheme of the synthesis procedure is shown in Fig. 2a.

2.3. Characterization of photocatalytic materials

The crystalline phase was characterized by the Rigaku Intelligent X-ray diffraction (XRD) system SmartLab (Rigaku Corporation, Tokyo, Japan). Scans were recorded in the 2θ range from 5° to 80°, with a speed of $2°{\cdot}min^{-1}$ and a step of 0.01°. Specific surface area and pore volume of the samples were evaluated through Brunauer-Emmett-Teller (BET) method by N_2 adsorption at 77 K (boiling point of liquid nitrogen) with the Micromeritics Gemini V apparatus (model 2365) (Norcross, GA, USA). Firstly a pretreatment at 200 °C for 2 h under nitrogen flow was performed. The light absorption properties were measured in the wavelength range from 200 nm to 800 nm by the ThermoScientific Evolution 220 spectrophotometer (Waltham, MA, USA) using barium sulfate as a standard reference. The bandgap energy was calculated using the Kubelka-Munk function, $(R)^{0.5}E_{ph}^{0.5}$ against E_{ph}, where E_{ph} is photon energy. The photocatalysts' surface morphology was measured by scanning electron microscopy (SEM) using SEM Microscope FEI Quanta FEG 250. Fourier-transform infrared spectroscopy (FTIR) analysis was performed using FTIR Nicolet iS10 (Thermo Fisher Scientific Waltham, MA, USA) spectrometer in the wavenumber from 400 to 4000 cm^{-1}. The surface chemistry of the samples was analyzed by X-ray photoelectron spectroscopy (XPS) using Escalab 250Xi multispectroscope (ThermoFisher Scientific). The spectroscope operates with a monochromatic AlKα X-ray source (spot size 650 μm). The high-resolution spectra were collected in the core-level binding energy range of Zn2p, Ti2p, C1s, and O1s, at pass energy of 20 eV. The charge compensation was provided by low-energy electron and Ar + ions bombardment throughout the measurement, with a final calibration at adventitious carbon C1s peak (284.8 eV). Spectral deconvolution was done using Avantage 5.9921 software (ThermoFisher Scientific). Transmission electron microscopy (TEM) and scanning transmission electron microscopy (STEM) analyses were carried out using Tecnai G2 200 kV and Thermo-Fisher Scientific Titan Themis Cs-corrector. Samples were dispersed in ethanol and subsequently placed on a carbon-coated copper grid.

The photoluminescence spectra (PL) and luminescence kinetic were registered using a spectrograph (Princeton Instr. Model Acton 2500i) coupled to a CCD streak camera (Hamamatsu Model C5680) operating in the 200–1100 nm spectral region with a temporal resolution of 20 ps. As an excitation source, a femtosecond laser was used (Coherent Model "Libra") equipped with an optical parametric amplifier (Light Conversion Model "OPerA").

Electrochemical impedance spectroscopy (EIS) measurements were performed using Potentiostat/Galvanostat Autolab PGSTAT204 (Metrohm Autolab) with a Na_2SO_4 (0.5 M) as an electrolyte. The photocatalytic materials were deposited on the carbon screen-printed electrodes with Ag/AgCl reference electrode (Metrohm Autolab). The diameter of the working electrode area was 4 mm. The AC voltage amplitude was 0.01 V, and the frequency ranged from 0.1 Hz to 100 kHz at 0 V *vs.* OCP (open circuit potential). The Mott Schottky analysis was performed to determine the flat band (F_b) potential of the Zn/Ti LDH. The EIS data were recorded from the anodic towards a cathodic direction. EIS data were recorded for the applied frequency of 1000 Hz in the potential range from 0 to −1.1 V vs. Ag/AgCl.

2.4. Photocatalytic activity

In a typical experiment, 0.05 g of the photocatalyst was dispersed in 25 cm^3 of 20 $mg{\cdot}dm^3$ acetaminophen or ibuprofen aqueous solution. The properties of both pharmaceuticals were summarized in Table 1S in the Supporting Materials. The photocatalytic process was carried out in a 25 cm^3 quartz reactor equipped with an air supply mode. A 300 W Xe lamp (LOT Oriel, Darmstadt, Germany) with the light flux in the UV range ($310\ nm < \lambda < 380\ nm$) equalled 30 $mW\ cm^{-2}$ was used as a light source, imitating the sunlight spectrum. Before the experiment, the photocatalyst suspension was kept in the dark for 30 min under continuous magnetic stirring to reach adsorption-desorption equilibrium before irradiation. During the photodegradation process, 1 cm^3 of the suspension was separated every 20 min using a 0.2 μm syringe filter. The photocatalytic processes were performed for 60 min. The rate of acetaminophen and ibuprofen degradation was monitored using reverse-phase high-performance liquid chromatograph Shimadzu UFLC LC-20AD (Kyoto, Japan) with photodiode array detector Shimadzu SPD-M20A. The measurements were performed at 45 °C and under isocratic flow conditions of 0.5 $cm^3\ min^{-1}$. A volume composition of the mobile phase of 70% acetonitrile, 29.5% water, and 0.5% orthophosphoric acid was applied to determine ibuprofen concentration, while 0.1% formic acid, 69.9% water, and 30% methanol to determine acetaminophen concentration. The total organic carbon (TOC) change in the photocatalytic process of acetaminophen and ibuprofen degradation was investigated using Shimadzu TOC Analyzer.

The additional experiments were performed in the model seawater to evaluate the effect of interfering ions on the efficiency of photocatalytic processes of acetaminophen and ibuprofen degradation. The composition of the model seawater was: 2.5% NaCl, 1.1% $MgCl_2$, 0.4% Na_2SO_4, 0.16% $CaCl_2$ in DI water (Wang et al., 2019). The concentration of ibuprofen or acetaminophen in model seawater was 20 mg/dm^3.

In the next step, the photocatalytic process was performed in the presence of scavengers to study the mechanism of acetaminophen and ibuprofen photodegradation. Ammonium oxalate was applied as holes scavenger (h^+), H_2O_2 for electrons (e^-), isopropyl alcohol for free hydroxyl radicals (·OH), and p-benzoquinone for superoxide radical anions ($\cdot O_2^-$).

3. Results and discussion

The SEM analysis was performed to show the morphology of MXene -$Ti_3C_2T_x$, Zn/Ti LDH, and Zn/Ti LDH-Ti_3C_2 composite. The formation of an accordion-like structure of MXene is presented in Fig. 1a. The obtained samples of pure LDH and Zn/Ti LDH-2.5% Ti_3C_2 composite present a flake-like morphology (Fig. 1b–c). However, there is no clearly visible difference between the morphology of the samples with various content of MXene (Fig. 1S in the Supporting Materials). The TEM images of Zn/Ti LDH-2.5% Ti_3C_2 (Fig. 1 d-e) confirmed the formation of Zn/Ti LDH flakes (brighter area) with and inclusions of MXene flakes (darker area). The TEM elemental mapping is presented in Fig. 2S in the Supporting Materials.

The XRD patterns of MAX, MXene and combined MXene/LDHs materials are presented in Fig. 2 b-c. After the etching of aluminium from Ti_3AlC_2, the synthesized $Ti_3C_2T_x$ showed the main diffraction peaks centred at $2\theta = 8.8°$, 18.1°, and 27.4°, corresponding to (002), (004), and (006) planes, indicating the MAX phase compound has been

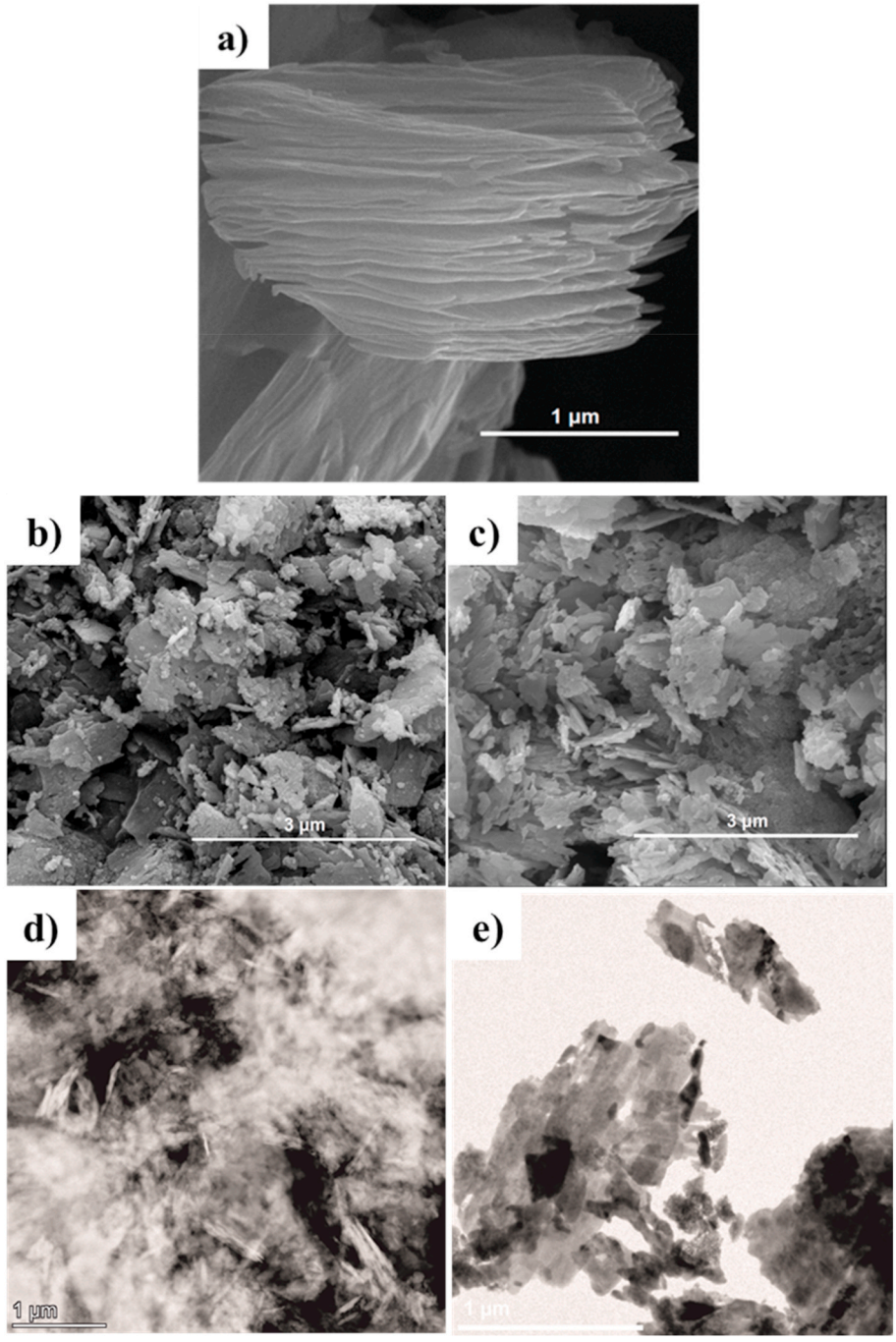

Fig. 1. SEM image of accordion-like $Ti_3C_2T_x$ (a), pure Zn/Ti LDH (b), Zn/Ti LDH-2.5% Ti_3C_2 (c), and TEM images of Zn/Ti LDH-2.5% Ti_3C_2 (d–e).

successfully transformed to Ti_3C_2 (Fig. 2a). The XRD analysis of $Ti_3C_2T_x$, which underwent a solvothermal reaction in the presence of urea, performed at 130 °C for 48 h, revealed the shifting of the MXene main diffraction peak to lower values of 2θ from 8.8° to 6.8° (Fig. 2b). This phenomenon of *d*-spacing increase may be related to the intercalation of urea and exfoliation during the solvothermal process (Yang et al., 2019). Furthermore, Zhao et al. stated that the presence of urea in the solvothermal reaction might prevent MXene from oxidation (Zhao et al., 2022).

Moreover, the X-ray diffraction (XRD) analysis confirmed the formation of Zn/Ti LDH, as shown in Fig. 2c. The narrow and symmetric peak characteristic for LDH at 2θ = 13.2° corresponding to the (003) reflection can be observed in all the obtained samples. The reflections of (006), (009), (110), and (113) can be assigned to LDH. For all composites materials, no diffraction signals corresponding to the MXene are noticed. A similar effect of no diffraction peaks identified for Ti_3C_2 was reported by Li et al. (2020) for Bi_3TaO_7/Ti_3C_2 composite, Cai et al. (2018) for Ag_3PO_4/Ti_3C_2, and Cheng et al. (2020) for $CdLa_2S_4/Ti_3C_2$ and Fang et al. (2019) for Ag_2WO_4/Ti_3C_2. This phenomenon is attributed to its ultra-thick surface property, low amount, and high dispersion. The incorporation of Ti_3C_2 did not affect the crystal structure of Zn/Ti LDH, excluding the influence of the crystal structure on photocatalytic activity. However, analyzing the crystallite size of Zn/TiLDH, it can be seen that the presence of MXene promotes the growth of LDHcrystallites, as presented in Table 2S in Supporting Materials.

The diffuse reflectance UV–vis spectroscopy (DR/UV–vis) was performed to investigate the optical absorption characteristics of the prepared materials. All results were normalized for better clarity and

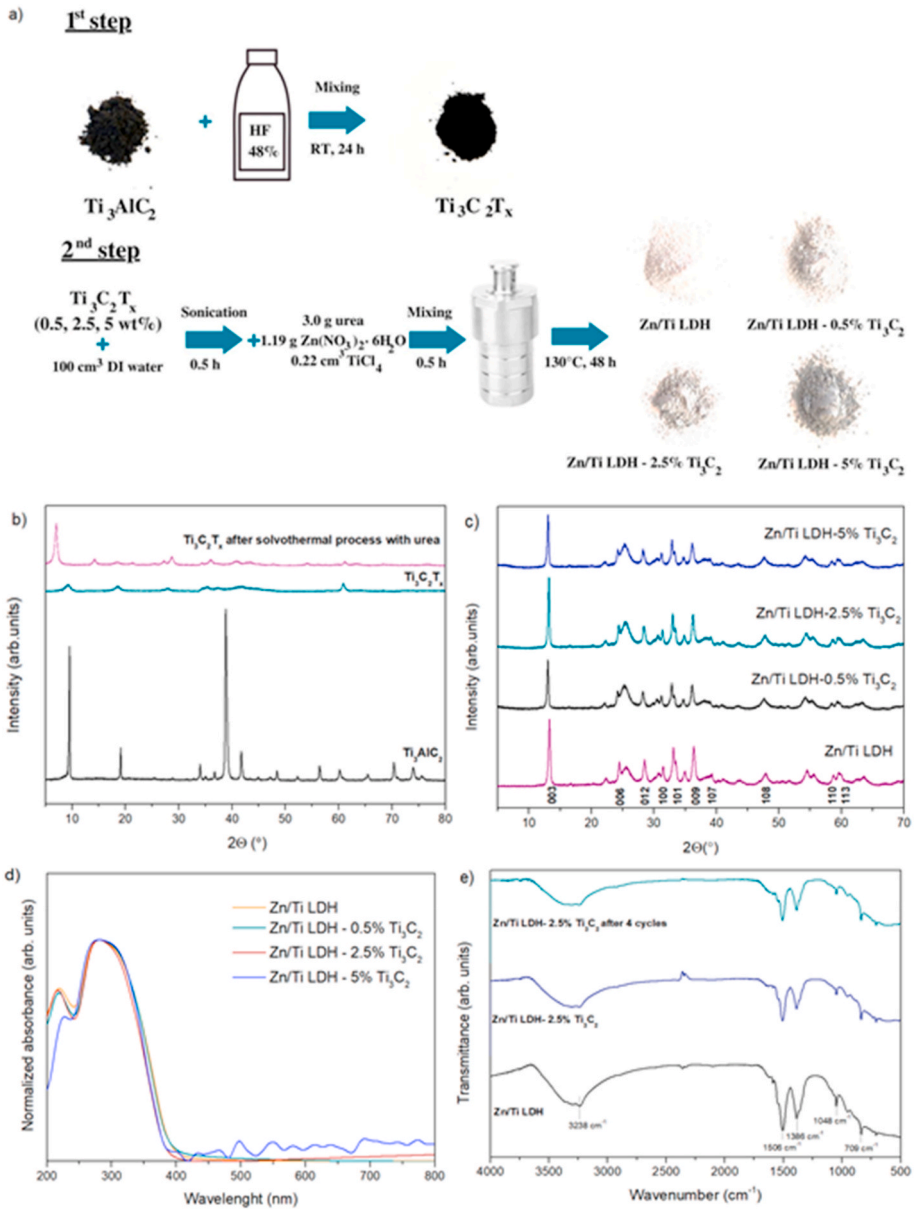

Fig. 2. Synthesis scheme (a), XRD diffractograms of Ti_3AlC_2, $Ti_3C_2T_x$, and $Ti_3C_2T_x$ after the solvothermal process with urea (b), XRD diffractograms of pure Zn/Ti LDH and Zn/Ti LDH-2.5%Ti_3C_2 (c), DR/UV–Vis spectra of Zn/Ti LDH and Zn/Ti LDH-Ti_3C_2 (d), and FTIR spectra of pure Zn/Ti LDH and Zn/Ti LDH-2.5%Ti_3C_2 (e).

comparison of the values. As shown in Fig. 2d, pure LDH exhibited strong absorption intensity only in the UV range with a threshold of about 400 nm. For the composite materials, a significant increase in the absorption in the range of 400–800 nm may be attributed to the presence of MXene and its absorption in the UV–Vis light range. It can be further observed by the gradually darker colour with higher content of MXene (inset in Fig. 2a). The Kubelka-Munk plots for obtained composites are presented in Fig. 3S in Supporting Materials. For samples containing MXene in the composition, the bandgap values were similar to pure LDH material. The physicochemical characteristics of pure MXene, Zn/TiLDH, and Zn/Ti LDH-Ti_3C_2 composites are presented in Table 2S in Supporting Materials. The BET surface area of pure MXene and Zn/Ti LDH was about 10.2 $m^2 \cdot g^{-1}$ and 129.4 $m^2 \cdot g^{-1}$, respectively. For the composite containing 0.5% of MXene, a slight decrease in surface area and pore volume was observed. The highest BET surface area of about 134.5 $m^2 \cdot g^{-1}$ was noticed for Zn/Ti LDH-5% Ti_3C_2.

Fig. 2e represents the FTIR spectra of pure Ti/Zn LDH and Zn/Ti LDH-2.5%Ti_3C_2. There is no difference between the spectra of pure LDH and the composite material. The strong, wide absorption band with a maximum at 3238 cm^{-1} is attributed to the O–H stretching mode. The characteristic signals at 1506 cm^{-1} and 1386 cm^{-1} are assigned to the interlayer carbonate anions (CO_3^{2-}) (Sun et al., 2019). Furthermore, weaker signals at 1048 cm^{-1} and 709 cm^{-1} are assigned to the carbonate and free carbonate ions (Egambaram et al., 2019).

The photoluminescence (PL) spectra of Zn/Ti-LDH and Zn/Ti-LDH-Ti_3C_2 photocatalysts were analyzed under 350 nm excitation wavelength (see Fig. 3a). The pure Zn/Ti-LDH showed a broad emission band with a maximum of about 450 nm, similar to Zn (Zhang et al., 2013) or Ti (Chowdhury and Bhattacharyya, 2015) doped LDH. The similar profiles of luminescence spectra of Zn or Ti-doped LDH powders suggest that the origin of the PL phenomenon may be the same. The emission in this region in the above-mentioned materials results from surface defects. The pure Zn/Ti-LDH catalyst shows strong photoluminescence attributed to the presence of either oxygen vacancies and/or defects in the LDH material. These defects resulting from the incorporation of Zn or Ti into the lattice have a strong impact on photocatalytic activity.

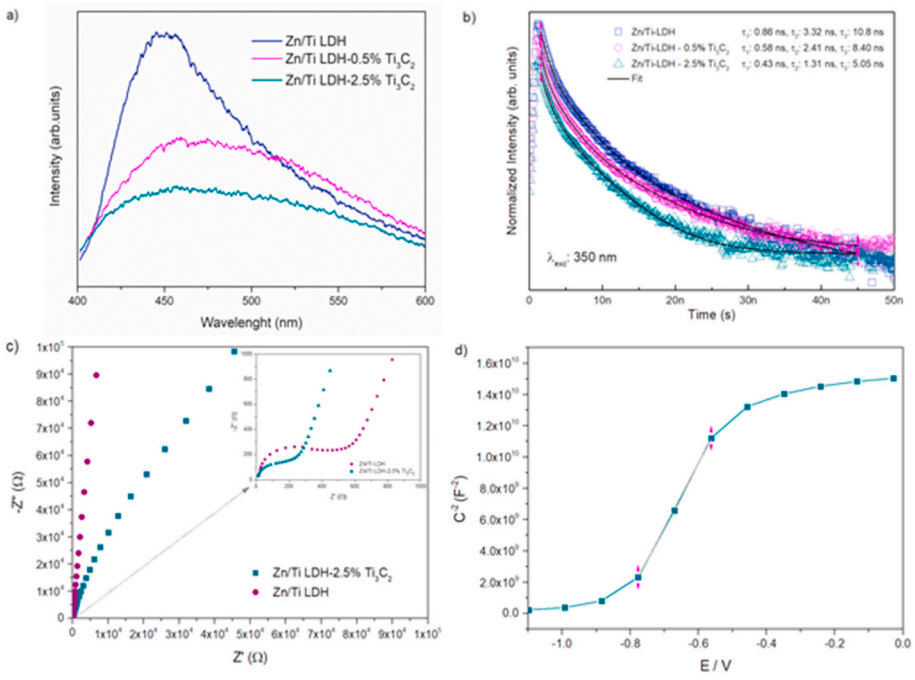

Fig. 3. Photoluminescence spectra (a), photoluminescence decay curves (b), EIS Nyquist plots (c) for Zn/Ti LDH-Ti_3C_2 composites, and Mott-Schottky plot (d) for sample Zn/Ti LDH.

Oxygen vacancies and defects are reported to bind the photo-induced electrons easily to form excitons, and PL signals may be easily observed. The broadened single-band emission spectrum observed instead of two or three narrower bands typical for emissions from semiconductor defects suggests the presence of hydroxyl groups and water molecules in LDH (Prestopino et al., 2019). For the composites of LDH with Ti_3C_2, the emission band is strongly broadened and slightly shifted toward longer wavelengths. The deconvolution of the broad band observed for the composite shows that it consists of three components. The first and third components (approx. 450 nm and sideband at 510 nm) are related to the emission from Zn/Ti-LDH, while the second component (observed at approx. 480 nm) overlapping the emission spectrum of the composite is assigned to the luminescence from surface defects in Ti_3C_2. The emission sum of both compounds leads to the broadening of the luminescence band, and the emission from Ti_3C_2 observed at longer wavelengths causes a slight redshift of the band. The lower PL intensity for composite material than pure Zn/Ti LDH results from a lower number of electron-hole recombination centres, which consequently increases the composites' photocatalytic efficiency.

As the luminescence decays showed a non-exponential character, three components were used for the correct fit of the curves (Fig. 3b). The multiexponential decays suggest that in the samples are different types of recombination centres. As the defects have different energy levels, they trap and release the carriers with variable transport rates. For composites, values of all three components (τ_1, τ_2, τ_3) are lower, and they decrease with the increase of Ti_3C_2 content, which is an effect of energy transfer between LDH and MXene and the distribution of the excitation energy between compounds and the emissions of both.

Fig. 3c shows the EIS Nyquist plot of the prepared photocatalysts. It can be seen that the combination of the LDH with MXene led to a decrease in the semicircle's diameter compared to pure Zn/Ti LDH, suggesting higher separation efficiency of the photo-induced charge carriers (Liu et al., 2020). As shown in Fig. 3d, Zn/Ti LDH-2.5% Ti_3C_2 composite Mott Schottky plot presented n-type characteristics. The potential of flat band edge position was recorded at −0.87 V vs. Ag/AgCl. This value was converted to a value of −0.58 V vs. NHE. Typically, for n-type semiconductors, the F_b potential is almost equal to the conduction band (CB) potential. Thus, the valence band (VB) edge of the composite was calculated as approx. 2.62 eV vs NHE.

The XPS analysis provided information about the oxidation states of elements in the composite material. The survey spectrum for Zn/Ti-LDH-2.5% Ti_3C_2 is presented in Fig. 4S in Supporting Materials. It can be seen that the photocatalyst consists of Zn, Ti, O, and C. The XPS Zn 2p, Ti 2p, O 1s, and C 1s regions for Zn/Ti-LDH-2.5% Ti_3C_2 are shown in Fig. 5S in Supporting Materials. The Zn 2p spectrum shows two characteristic peaks at 1022 eV and 1044 eV attributed to Zn $2p_{3/2}$ and $2p_{1/2}$, respectively, corresponding to the occurrence of zinc in the form of Zn^{2+} in LDH structure (Liu et al., 2021b; Li et al., 2019b). The Ti 2p spectrum may be deconvoluted in four doublet pairs at 455 eV, 457 eV, 457.5 eV, and 459 eV($2p_{3/2}$), which correspond to Ti–C, C–Ti–O, Ti^{3+}, and Ti^{4+}, respectively. The Ti–C and C–Ti–O are related to the presence of MXene (Lu et al., 2021). The signal from Ti^{3+} may be attributed to the Ti_3C_2 or defects in the lattice of Zn/Ti LDH. The formation of Ti^{3+} defects was also noticed in the studies presented by Zhao et al., 2013, 2014 for Ni/Ti LDH and Zn/Ti LDH. The formation of Ti^{3+} defects in the Zn/Ti LDH lattice results from removing oxygen atoms from the surface. The presence of such surface defects results in more oxygen defects, which influence the electronic properties and enhance the separation of electron-hole pairs. Furthermore, it has also been reported that the electron trapped on the Ti^{3+} are able to form superoxide anion radicals from surface-absorbed oxygen (Zhao et al., 2013, 2014). The high-resolution C 1s spectrum is divided into five signals at approximately 283 eV, 284 eV, 285 eV, 286.5 eV, and 289 eV corresponding to Ti–C, C–Ti–O, and C–C/C═C in the MXene structure, and in C–O and C═O bonds in carbonate groups (Ahmed et al., 2016). In the O 1s spectrum, six signals occurred at 528 eV, 529 eV, 530.5 eV, 531.5 eV, 533 eV, and 534 eV, attributed to adsorbed oxygen, metal-oxide bonds, CO_3^{2-}, metal-hydroxide bonds, C═O, and H_2O, respectively (Zheng et al., 2019; Chubar et al., 2013).

The photocatalytic activity of Zn/Ti LDHand Zn/Ti LDH-Ti_3C_2 composites was evaluated in reactions of pharmaceuticals degradation under simulated solar light. Fig. 4a–d and Tables 3S–5S in the Supporting Materials present the results of acetaminophen and ibuprofen removal by direct photolysis and in the presence of photocatalytic material. As can be seen, the photolysis of acetaminophen after 60 min of irradiation was only about 11%. On the contrary, ibuprofen

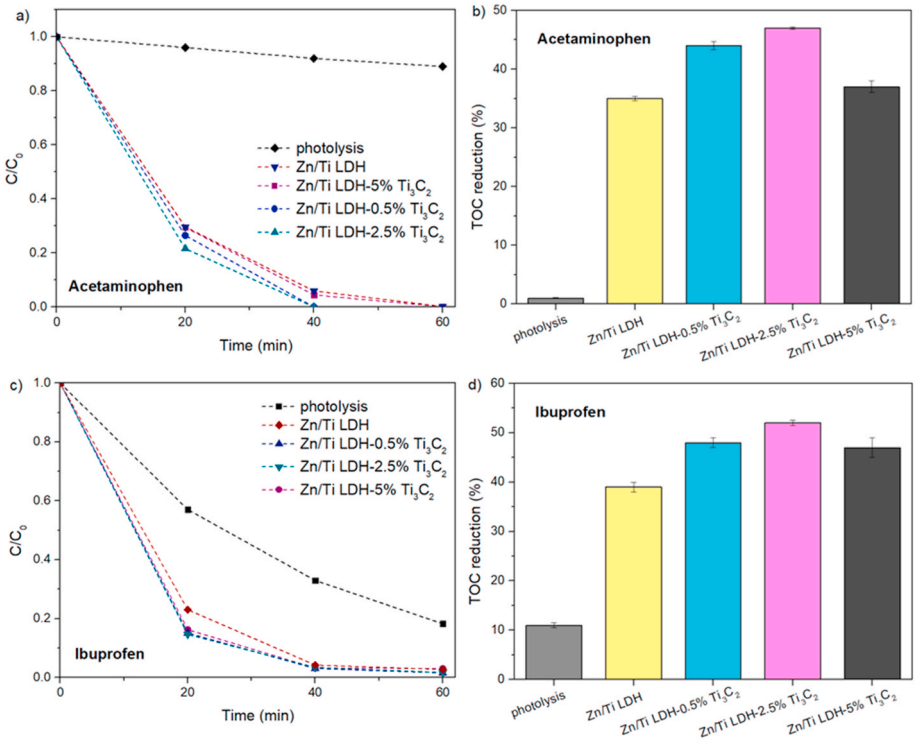

Fig. 4. Efficiency of acetaminophen degradation (C/C_0) (a), TOC reduction (%) for ACT (b), efficiency of ibuprofen degradation (C/C_0) (c) TOC reduction (%) for IBP (d) Zn/Ti LDH and Zn/Ti LDH-Ti_3C_2 photocatalysts.

photodegradation under the same conditions reached about 80%. However, the total organic carbon analysis revealed that after the photolysis of acetaminophen and ibuprofen, the reduction of TOC was equal to 1% and 11.5%, respectively. The application of pure Zn/Ti LDH photocatalyst increased the TOC removal by 34% for ACT degradation and by 27.5% for IBP removal, compared to photolysis. Furthermore, it was observed that coupling of Zn/Ti LDH with the MXene compound led to improved photocatalytic degradation and mineralization of both pharmaceuticals. When the amount of Ti_3C_2 in the composite was 2.5%, the rate constant of acetaminophen degradation increased from 8.1 to 12.8 $min^{-1}{\cdot}10^{-2}$, while TOC reduction increased from 35% to 47% compared to pure Zn/Ti LDH. For this composite, 100% of acetaminophen was removed within 40 min of UV–vis irradiation. In the case of IBP degradation, the rate constant increased from 5.8 to 7.1 $min^{-1}{\cdot}10^{-2}$, while TOC reduction increased from 39% to 52% compared to pure Zn/Ti LDH. Almost complete degradation of IBP was observed within 60 min. The decrease in the activity with the higher content of MXene may be related to the overloading of the photocatalyst surface. The increasing amount of MXene could shield the light absorption of the photocatalyst and thus inhibit photocatalytic activity. A similar Ti_3C_2 overloading effect was observed by Huang et al. (2019) for Bi_2WO_6/Ti_3C_2, Que et al. (2022) for $FAPbBr_3/Ti_3C_2$ composite or Liu et al. (2021c) for C_3N_4/Ti_3C_2 material.

To evaluate the effect of interfering ions on the efficiency of ACT and IBP photocatalytic degradation, the photodegradation of pharmaceuticals was performed in the model seawater containing the following ions: Na^+, Ca^{2+}, Mg^{2+}, Cl^-, and SO_4^{2-}. Some previously reported results showed that inorganic anions such as Cl^- ion in water might reduce photocatalytic activity due to the fact that induced hydroxyl radicals are scavenged by chloride ions or Cl^- can be adsorbed on the surface of photocatalyst and block the active sites (Makita and Harata, 2008; Porcar-Santos et al., 2020). As shown in Fig. 5a–b and in Table 6S in the Supporting Materials in the present study, the degradation efficiency of both pharmaceuticals was unaffected by interfering inorganic ions. This is an important fact about the viability of photocatalytic water treatments using Zn/Ti LDH-2.5%Ti_3C_2 in saline water samples.

In order to elucidate the photocatalytic mechanism, experiments with scavengers for the detection of reactive oxygen species (ROS) participating in the photodegradation process of ACT and IBP were performed (Fig. 5c–d). The content of each scavenger was equal to 0.03 mmol (10-fold concentration of contaminant). Performed experiments showed that the mechanisms of degradation of ACT and IBP are different. In the case of ACT, the inhibitory effect of ammonium oxalate was weak, indicating that holes did not play a significant role in the degradation process. The highest inhibition effect was noticed for p-benzoquinone, suggesting that superoxide anion radicals appear to be the most likely ROS in ACT degradation (Wang et al., 2021b; Fan et al., 2018). Meanwhile, for IBP, the main species involved in the photocatalytic process were holes and hydroxyl radicals due to the limitation of the reaction that occurred in the presence of ammonium oxalate and isopropanol, respectively. These results are consistent with the previous studies of Jiménez-Salcedo et al. (2021) and Sá et al. (2021), who observed that holes are major ROS involved in the degradation of IBP. Also, Liu et al. (Liu et al., 1016) confirmed that holes and hydroxyl radicals are responsible for IBP degradation using niobium-doped TiO_2 nanotubes.

Furthermore, the excellent stability of the prepared LDH/MXene composite was confirmed in the four subsequent photocatalytic cycles of acetaminophen degradation, as shown in Fig. 5e. After the fourth cycle, the efficiency of pollutant removal still reached 100% within 40 min, thus suggesting the high potential of photocatalyst for reusability. Also, the TOC reduction remains unchanged after repetitive photocatalytic cycles. Furthermore, the FTIR (Fig. 2e), TEMTEM (Fig. 3S in Supporting Materials), and XPS (Fig. 5S in Supporting Materials) analyses after the photocatalytic processes did not show any changes in the structure of the photocatalyst.

A schematic illustration of the photocatalytic mechanism of IBP and ACT degradation in the presence of Zn/Ti LDH-2.5% Ti_3C_2 photocatalyst is proposed and presented in Fig. 6. Photogenerated electrons are transferred and accumulated by the MXene, inhibiting the

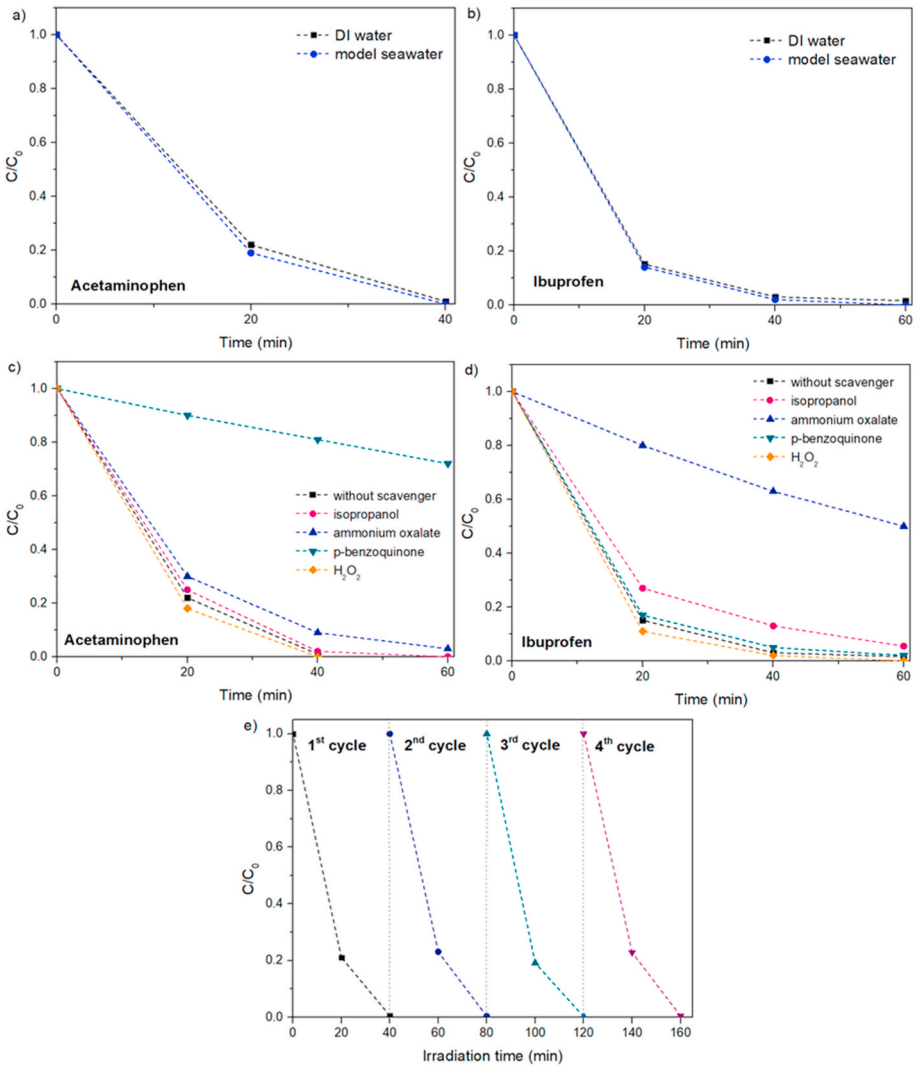

Fig. 5. ACT photocatalytic degradation in DI water and model seawater for Zn/Ti LDH-2.5%Ti_3C_2 (a), ibuprofen degradation in DI water and model seawater for Zn/Ti LDH-2.5%Ti_3C_2 (b), the effect of scavengers on the ACT photocatalytic degradation (c) and IBP degradation for Zn/Ti LDH-2.5%Ti_3C_2 (d), cycling test of the ACT photocatalytic degradation for Zn/Ti LDH-2.5%Ti_3C_2 (e).

recombination of electron-hole pairs. Meanwhile, based on the CB and VB location, the sample Zn/Ti LDH-2.5% Ti_3C_2 may oxidize water molecules to hydroxyl radicals as well as reduce oxygen into superoxide anion radicals.

The performance of the Zn/Ti LDH-2.5% Ti_3C_2 composite was compared with the previously reported photocatalysts used for photodegradation of ACT or IBP, and the results are shown in Table 1. It was found that the Zn/Ti LDH-Ti_3C_2 photocatalyst prepared in our work has excellent performance compared with other materials, especially considering the high degradation efficiency of both pharmaceuticals within 60 min under simulated solar light.

4. Conclusions

In summary, for the first time, the series of novel composites of Zn/Ti LDH coupled with MXene-$Ti_3C_2T_x$ were successfully synthesized and characterized. The important role of the MXene compound as a co-catalyst in photocatalytic water treatment was proven. Specifically, the composite with optimal content of $Ti_3C_2T_x$ equal to 2.5% exhibited superior activity towards degradation of acetaminophen (100% within 40 min) and ibuprofen (99.7% within 60 min), frequently detected pharmaceuticals in surface waters. The presence of MXene - Ti_3C_2 in the composite structure facilitates electron transfer inhibiting the electron-hole recombination process. So far, there are only a few studies concerning the application of LDH/MXene composites in photocatalysis. Thus, the findings presented in this paper enriched the possible application of LDH/MXene photocatalyst for water purification. Furthermore, the essential is the potential use of composite Zn/Ti LDH-2.5% Ti_3C_2 for saline water treatment, where activity was unaffected by interfering inorganic ions, which may have great importance in the environmental aspects. Besides, this composite also shows excellent recycling stability with no changes in photocatalytic efficiency and the material properties in the subsequent cycles of photocatalytic degradation. Finally, we proposed the mechanism of pharmaceuticals degradation based on the trapping experiments with scavengers of ROS, bandgap calculation, and Mott Schottky analysis. The main reactive oxygen species involved in photocatalytic degradation of acetaminophen are superoxide anion radicals (O_2^-), while for ibuprofen holes (h^+) and hydroxyl radicals (OH). Overall, the findings presented in this studies enriched the LDH/MXene photocatalysts, demonstrating highly prospective strategy for pharmaceuticals treatment under solar light.

Author contributions

Conceptualization, AZ-J.; Synthesis, AG; Formal analysis, AG, IW, PG, JR, JK; Funding acquisition, AZ-J.; Investigation, AG; Methodology,

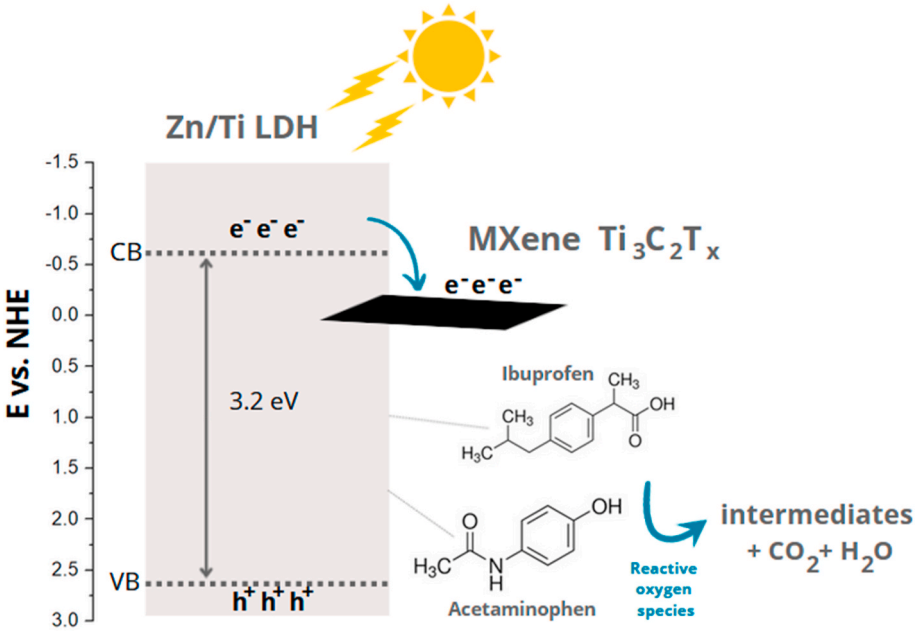

Fig. 6. Schematic illustration of the possible mechanism of ACT and IBP degradation in the presence of Zn/Ti LDH-Ti_3C_2 photocatalyst.

Table 1
The comparison of this work with results presented in recent related papers.

Photocatalyst	Catalyst loading (g/dm^3)	Pharmaceutical concentration (mg/dm^3)	Light source	Degradation efficiency	Ref.
TiO_2/polyethersulphone	n.d. (film - 320 cm^2)	ACT, 10	UV-A lamp	80% in 7 h	Chijioke-Okere et al. (2021)
Sr@TiO_2/UiO-66-NH_2	0.25	ACT, 5	Xe lamp with a 320 nm cut-off filter	90% in 4 h	Wang et al. (2022)
carbon xerogel/TiO_2	2	ACT, 25	Hg lamp	96% in 4 h	da Cunha et al. (2021)
noble metal-decorated NH_2-MIL-125	0.25	ACT, 5	Xe lamp with a 290 nm cut off filter	100% in 3 h	Muelas-Ramos et al. (2021)
α-$SnWO_4$/UiO-66(NH_2)/g-C_3N_4	0.5	IBP, 10	Xe lamp	95% in 2 h	Wei et al. (2021)
biochar–$ZnAl_2O_4$	1	IBP, 20	Hg lamp	100% in 2 h	Siara et al. (2022)
Ag/Bi-decorated BiOBr	0.3	IBP, 20	Xe lamp	92.3% within 1 h	Qin et al. (2022)
FeO supported on modified Iranian clinoptilolite	0.3	IBP, 25	Xe lamp	99.8% in 3 h	Mohadesi et al. (2022)
Zn/Ti LDH-2.5%Ti_3C_2	2	ACT, 20/IBP, 20	Xe lamp	100% in 40 min/99.7% in 1 h	this work

AZ-J; Project administration, AZ-J.; Writing – original draft, AG, AZ-J; Writing – review & editing, AG, AZ-J, IW

Declaration of competing interest

The authors declare that they have no known competing financial interests or personal relationships that could have appeared to influence the work reported in this paper.

Data availability

Data will be made available on request.

Acknowledgements

The research was financially supported by Polish National Science Centre (Grant No. NCN 2018/30/E/ST5/00845).

Appendix A. Supplementary data

Supplementary data to this article can be found online at https://doi.org/10.1016/j.chemosphere.2022.136191.

References

Ahmed, B., Anjum, D.H., Hedhili, M.N., Gogotsi, Y., Alshareef, H.N., 2016. H2O2 assisted room temperature oxidation of Ti2C MXene for Li-ion battery anodes. Nanoscale. https://doi.org/10.1039/c6nr00002a.

Akpotu, S.O., Oseghe, E.O., Ayanda, O.S., Skelton, A.A., Msagati, T.A.M., Ofomaja, A.E., 2019. Photocatalysis and biodegradation of pharmaceuticals in wastewater: effect of abiotic and biotic factors. Clean Technol. Environ. Policy 21, 1701–1721. https://doi.org/10.1007/s10098-019-01747-4.

Article, R., Rao, a V.P., Umabala, a M., Suresh, P., 2015. Non-TiO_2 based photocatalysts for remediation of hazardous organic pollutants under green technology-present status. Rev. 4, 1145–1172.

Branchet, P., Arpin-Pont, L., Piram, A., Boissery, P., Wong-Wah-Chung, P., Doumenq, P., 2021. Pharmaceuticals in the marine environment: what are the present challenges in their monitoring? Sci. Total Environ. 766, 142644 https://doi.org/10.1016/j.scitotenv.2020.142644.

Cai, T., Wang, L., Liu, Y., Zhang, S., Dong, W., Chen, H., Yi, X., Yuan, J., Xia, X., Liu, C., Luo, S., 2018. Ag3PO4/Ti3C2 MXene interface materials as a Schottky catalyst with enhanced photocatalytic activities and anti-photocorrosion performance. Appl. Catal. B Environ. 239, 545–554. https://doi.org/10.1016/j.apcatb.2018.08.053.

Chen, W., Han, B., Xie, Y., Liang, S., Deng, H., Lin, Z., 2020. Ultrathin Co-Co LDHs nanosheets assembled vertically on MXene: 3D nanoarrays for boosted visible-light-driven CO2 reduction. Chem. Eng. J. 391, 123519 https://doi.org/10.1016/j.cej.2019.123519.

Cheng, L., Chen, Q., Li, J., Liu, H., 2020. Boosting the photocatalytic activity of CdLa2S4 for hydrogen production using Ti3C2 MXene as a co-catalyst. Appl. Catal. B Environ. 267, 118379 https://doi.org/10.1016/j.apcatb.2019.118379.

Chijioke-Okere, M.O., Mohd Hir, Z.A., Ogukwe, C.E., Njoku, P.C., Abdullah, A.H., Oguzie, E.E., 2021. TiO2/Polyethersulphone films for photocatalytic degradation of acetaminophen in aqueous solution. J. Mol. Liq. 338, 116692 https://doi.org/10.1016/j.molliq.2021.116692.

Chowdhury, P.R., Bhattacharyya, K.G., 2015. Ni/Ti layered double hydroxide: synthesis, characterization and application as a photocatalyst for visible light degradation of aqueous methylene blue. Dalton Trans. 15 https://doi.org/10.1039/C5DT00257E.

Chubar, N., Gerda, V., Megantari, O., Mičušík, M., Omastova, M., Heister, K., Man, P., Fraissard, J., 2013. Applications versus properties of Mg–Al layered double hydroxides provided by their syntheses methods: alkoxide and alkoxide-free sol–gel syntheses and hydrothermal precipitation. Chem. Eng. J. 234, 284–299. https://doi.org/10.1016/j.cej.2013.08.097.

da Cunha, R., do Carmo Batista, W.V.F., de Oliveira, H.L., dos Santos, A.C., dos Reis, P. M., Borges, K.B., Martelli, P.B., Furtado, C.A., de Fátima Gorgulho, H., 2021. Carbon Xerogel/TiO2 composites as photocatalysts for acetaminophen degradation. J. Photochem. Photobiol., A 412, 113248. https://doi.org/10.1016/j.jphotochem.2021.113248.

Desbiolles, F., Malleret, L., Tiliacos, C., Wong-Wah-Chung, P., Laffont-Schwob, I., 2018. Occurrence and ecotoxicological assessment of pharmaceuticals: is there a risk for the Mediterranean aquatic environment? Sci. Total Environ. 639, 1334–1348. https://doi.org/10.1016/j.scitotenv.2018.04.351.

Dey, A., Sandre, V., Marangoni, D.G., Ghosh, S., 2018. Interaction between a nonsteroidal anti-inflammatory drug (ibuprofen) and an anionic surfactant (AOT) and effects of salt (NaI) and hydrotrope (4-4-4). J. Phys. Chem. B 122, 3974–3987. https://doi.org/10.1021/acs.jpcb.8b00687.

Egambaram, O.P., Pillai, S.K., Lategan, M., Ray, S.S., 2019. Nanostructured Zn-Ti layered double hydroxides with reduced photocatalytic activity for sunscreen application. J. Nanoparticle Res. 21 https://doi.org/10.1007/s11051-019-4488-3.

Fan, G., Zheng, X., Luo, J., Peng, H., Lin, H., Bao, M., Hong, L., Zhou, J., 2018. Rapid synthesis of Ag/AgCl@ZIF-8 as a highly efficient photocatalyst for degradation of acetaminophen under visible light. Chem. Eng. J. 351, 782–790. https://doi.org/10.1016/j.cej.2018.06.119.

Fang, Y., Cao, Y., Chen, Q., 2019. Synthesis of an Ag2WO4/Ti3C2 Schottky composite by electrostatic traction and its photocatalytic activity. Ceram. Int. 45, 22298–22307. https://doi.org/10.1016/j.ceramint.2019.07.256.

Guo, X., Zhang, F., Evans, D.G., Duan, X., 2010. Layered double hydroxide films: synthesis, properties and applications, Chem. Commun. Now. 46, 5197–5210. https://doi.org/10.1039/c0cc00313a.

Hao, C., Wu, Y., An, Y., Cui, B., Lin, J., Li, X., Wang, D., Jiang, M., Cheng, Z., Hu, S., 2019. Interface-coupling of CoFe-LDH on MXene as high-performance oxygen evolution catalyst. Mater. Today Energy 12, 453–462. https://doi.org/10.1016/j.mtener.2019.04.009.

Huang, G., Li, S., Liu, L., Zhu, L., Wang, Q., 2019. Ti3C2 MXene-modified Bi2WO6 nanoplates for efficient photodegradation of volatile organic compounds. Appl. Surf. Sci. https://doi.org/10.1016/j.apsusc.2019.144183.

Jiménez-Salcedo, M., Monge, M., Tena, M.T., 2021. Combination of au-ag plasmonic nanoparticles of varied compositions with carbon nitride for enhanced photocatalytic degradation of ibuprofen under visible light. Materials 14. https://doi.org/10.3390/ma14143912.

Klementova, S., Kahoun, D., Doubkova, L., Frejlachova, K., Dusakova, M., Zlamal, M., 2017. Catalytic photodegradation of pharmaceuticals-homogeneous and heterogeneous photocatalysis. Photochem. Photobiol. Sci. 16, 67–71. https://doi.org/10.1039/c6pp00164e.

Li, M., Fang, L., Zhou, H., Wu, F., Lu, Y., Luo, H., Zhang, Y., Hu, B., 2019a. Three-dimensional porous MXene/NiCo-LDH composite for high performance non-enzymatic glucose sensor. Appl. Surf. Sci. 495 https://doi.org/10.1016/j.apsusc.2019.143554.

Li, Y., Xu, J., Liu, Z., Yu, H., 2019b. Performance of amorphous CoSx/oxygen vacancies ZnO heterojunction photocatalytic hydrogen evolution. J. Mater. Sci. Mater. Electron. 30, 246–258. https://doi.org/10.1007/s10854-018-0287-3.

Li, K., Lu, X., Zhang, Y., Liu, K., Huang, Y., Liu, H., 2020. Bi3TaO7/Ti3C2 heterojunctions for enhanced photocatalytic removal of water-borne contaminants. Environ. Res. 185, 109409. https://doi.org/10.1016/j.envres.2020.109409.

Liang, C., Lan, Z., Zhang, X., Liu, Y., 2016. Mechanism for the primary transformation of acetaminophen in a soil/water system. Water Res. 98, 215–224. https://doi.org/10.1016/j.watres.2016.04.027.

W. Liu, W. Zhang, M. Liu, P. Du, C. Dang, J. Liang, Y. Li, Fabrication of Niobium Doped Titanate Nanoflakes with Enhanced Visible-Light-Driven Photocatalytic Activity for Efficient Ibuprofen Degradation https://doi.org/10.1016/j.cclet.2019.07.050.

Liu, Y., Zeng, X., Easton, C.D., Li, Q., Xia, Y., Yin, Y., Hu, X., Hu, J., Xia, D., McCarthy, D. T., Deletic, A., Sun, C., Yu, J., Zhang, X., 2020. An in situ assembled –TiO2 vertical heterojunction for enhanced Z-scheme photocatalytic activity. Nanoscale 12, 8775. https://doi.org/10.1039/d0nr01611j.

Liu, G., Feng, M., Tayyab, M., Gong, J., Zhang, M., Yang, M., Lin, K., 2021a. Direct and efficient reduction of perfluorooctanoic acid using bimetallic catalyst supported on carbon. J. Hazard Mater. 412, 125224 https://doi.org/10.1016/j.jhazmat.2021.125224.

Liu, Y., Zhu, Q., Tayyab, M., Zhou, L., Lei, J., Zhang, J., 2021b. Single-atom Pt loaded zinc vacancies ZnO-ZnS induced type-V electron transport for efficiency photocatalytic H2 evolution. Solar RRL 5, 2100536. https://doi.org/10.1002/solr.202100536.

Liu, W., Sun, M., Ding, Z., Gao, B., Ding, W., 2021c. Ti3C2 MXene embellished g-C3N4 nanosheets for improving photocatalytic redox capacity. J. Alloys Compd. 877, 160233 https://doi.org/10.1016/j.jallcom.2021.160223.

Liu, Y., Chen, S., Li, K., Wang, J., Chen, P., Wang, H., Li, J., Dong, F., 2022. Promote the activation and ring opening of intermediates for stable photocatalytic toluene degradation over Zn-Ti-LDH. J. Colloid Interface Sci. 606, 1435–1444. https://doi.org/10.1016/j.jcis.2021.08.146.

Lu, C., Li, A., Li, G., Yan, Y., Zhang, M., Yang, Q., Zhou, W., Guo, L., 2021. S-decorated porous Ti3C2 MXene combined with in situ forming Cu2Se as effective shuttling interrupter in Na–Se batteries. Adv. Mater. 33 https://doi.org/10.1002/adma.202008414.

Ma, Y., Xu, D., Chen, W., Tang, Y., Wang, X., Li, L., Wang, J., 2022. Oxygen-vacancy-embedded 2D/2D NiFe-LDH/MXene Schottky heterojunction for boosted photodegradation of norfloxacin. Appl. Surf. Sci. 572, 151432 https://doi.org/10.1016/j.apsusc.2021.151432.

Makita, M., Harata, A., 2008. Photocatalytic decolorization of rhodamine B dye as a model of dissolved organic compounds: influence of dissolved inorganic chloride salts in seawater of the Sea of Japan. Chem. Eng. Process. Process Intensif. 47, 859–863. https://doi.org/10.1016/j.cep.2007.01.036.

Mohadesi, M., Gouran, A., Seifi, K., 2022. Removal of ibuprofen from synthetic wastewater using photocatalytic method in the presence of FeO photocatalyst supported on modified Iranian clinoptilolite. Environ. Sci. Pollut. Res. 29, 34338–34348. https://doi.org/10.1007/s11356-021-18153-3.

Motlagh, P.Y., Khataee, A., Hassani, A., Sadeghi Rad, T., 2020. ZnFe-LDH/GO nanocomposite coated on the glass support as a highly efficient catalyst for visible light photodegradation of an emerging pollutant. J. Mol. Liq. 302, 112532 https://doi.org/10.1016/j.molliq.2020.112532.

Muelas-Ramos, V., Belver, C., Rodriguez, J.J., Bedia, J., 2021. Synthesis of noble metal-decorated NH2-MIL-125 titanium MOF for the photocatalytic degradation of acetaminophen under solar irradiation. Separ. Purif. Technol. 272, 118896 https://doi.org/10.1016/j.seppur.2021.118896.

Naz, A., Chowdhury, A., Mishra, B.K., 2021. Applications of microbes in bioremediation of point source pollutants from wastewater. IOP Conf. Ser. Earth Environ. Sci. 796 https://doi.org/10.1088/1755-1315/796/1/012039.

Pemberthy M, D., Padilla, Y., Echeverri, A., Peñuela, G.A., 2020. Monitoring pharmaceuticals and personal care products in water and fish from the Gulf of Urabá, Colombia. Heliyon 6. https://doi.org/10.1016/j.heliyon.2020.e04215.

Peña-Guzmán, C., Ulloa-Sánchez, S., Mora, K., Helena-Bustos, R., Lopez-Barrera, E., Alvarez, J., Rodriguez-Pinzón, M., 2019. Emerging pollutants in the urban water cycle in Latin America: a review of the current literature. J. Environ. Manag. 237, 408–423. https://doi.org/10.1016/j.jenvman.2019.02.100.

Phong Vo, H.N., Le, G.K., Hong Nguyen, T.M., Bui, X.T., Nguyen, K.H., Rene, E.R., Vo, T. D.H., Thanh Cao, N.D., Mohan, R., 2019. Acetaminophen micropollutant: historical and current occurrences, toxicity, removal strategies and transformation pathways in different environments. Chemosphere 236, 124391. https://doi.org/10.1016/j.chemosphere.2019.124391.

Porcar-Santos, O., Cruz-Alcalde, A., López-Vinent, N., Zanganas, D., Sans, C., 2020. Photocatalytic degradation of sulfamethoxazole using TiO2 in simulated seawater: evidence for direct formation of reactive halogen species and halogenated by-products. Sci. Total Environ. 736, 139605 https://doi.org/10.1016/j.scitotenv.2020.139605.

Prestopino, G., Arrabito, G., Generosi, A., Mattoccia, A., Paci, B., Perez, G., Verona-Rinati, G., Medaglia, P.G., 2019. Emerging switchable ultraviolet photoluminescence in dehydrated Zn/Al layered double hydroxide nanoplatelets. Sci. Rep. 9, 11498 https://doi.org/10.1038/s41598-019-48012-8.

Priya, A.K., Gnanasekaran, L., Rajendran, S., Qin, J., Vasseghian, Y., 2022. Occurrences and removal of pharmaceutical and personal care products from aquatic systems using advanced treatment- A review. Environ. Res. 204, 112298 https://doi.org/10.1016/j.envres.2021.112298.

Qin, M., Jin, K., Li, X., Wang, R., Li, Y., Wang, H., 2022. Novel highly-active Ag/Bi dual nanoparticles-decorated BiOBr photocatalyst for efficient degradation of ibuprofen. Environ. Res. 206, 112628 https://doi.org/10.1016/j.envres.2021.112628.

Que, M., Cai, W., Zhao, Y., Yang, Y., Zhang, B., Yun, S., Chen, J., Zhu, G., 2022. 2D/2D Schottky heterojunction of in-situ growth FAPbBr3/Ti3C2 composites for enhancing photocatalytic CO2 reduction. J. Colloid Interface Sci. 610, 538–545. https://doi.org/10.1016/j.jcis.2021.11.094.

Rasheed, T., Shafi, S., Bilal, M., Hussain, T., Sher, F., Rizwan, K., 2020. Surfactants-based remediation as an effective approach for removal of environmental pollutants—a review. J. Mol. Liq. 318 https://doi.org/10.1016/j.molliq.2020.113960.

Razzaq, A., Ali, S., Asif, M., In, S., 2020. Layered Double Hydroxide (LDH) Based Photocatalytic CO_2 Conversion.

Ruggeri, G., Ghigo, G., Maurino, V., Minero, C., Vione, D., 2013. Photochemical transformation of ibuprofen into harmful 4-isobutylacetophenone: pathways, kinetics, and significance for surface waters. Water Res. 47, 6109–6121. https://doi.org/10.1016/j.watres.2013.07.031.

Sá, A.S., Feitosa, R.P., Honório, L., Peña-Garcia, R., Almeida, L.C., Dias, J.S., Brazuna, L. P., Tabuti, T.G., Triboni, E.R., Osajima, J.A., da Silva-Filho, E.C., 2021. A brief photocatalytic study of zno containing cerium towards ibuprofen degradation. Materials 14. https://doi.org/10.3390/ma14195891.

Shao, M., Han, J., Wei, M., Evans, D.G., Duan, X., 2011. The synthesis of hierarchical Zn-Ti layered double hydroxide for efficient visible-light photocatalysis. Chem. Eng. J. 168, 519–524. https://doi.org/10.1016/j.cej.2011.01.016.

Siara, S., Elvis, C., Harishkumar, R., Velayudhaperumal Chellam, P., 2022. ZnAl2O4 supported on lychee-biochar applied to ibuprofen photodegradation. Mater. Res. Bull. 145, 111530 https://doi.org/10.1016/j.materresbull.2021.111530.

Singh, T., Awasthi, G., Tiwari, Y., 2021. Recruiting endophytic bacteria of wetland plants to phytoremediate organic pollutants. Int. J. Environ. Sci. Technol. https://doi.org/10.1007/s13762-021-03476-y.

Sousa, J.C.G., Ribeiro, A.R., Barbosa, M.O., Pereira, M.F.R., Silva, A.M.T., 2018. A review on environmental monitoring of water organic pollutants identified by EU

guidelines. J. Hazard Mater. 344, 146–162. https://doi.org/10.1016/j.jhazmat.2017.09.058.
Sun, D., Chi, D., Yang, Z., Xing, Z., Yin, J., Li, Z., Zhu, Q., Zhou, W., 2019. Mesoporous g-C3N4/Zn–Ti LDH laminated van der Waals heterojunction nanosheets as remarkable visible-light-driven photocatalysts. Int. J. Hydrogen Energy 44, 16348–16358. https://doi.org/10.1016/j.ijhydene.2019.04.275.
Tayyab, M., Liu, Y., Min, S., Irfan, R.M., Zhu, Q., Zhou, L., Lei, J., Zhang, J., 2022. Simultaneous hydrogen production with the selective oxidation of benzyl alcohol to benzaldehyde by a noble-metal-free photocatalyst VC/CdS nanowires. Chin. J. Catal. 43, 1165–1175. https://doi.org/10.1016/S1872-2067(21)63997-9.
Wang, T., Li, Y., hao Pan, J., ling Zhang, Y., guang Wu, L., ying Dong, C., juan Li, C., 2019. Alcohol solvothermal reduction for commercial P25 to harvest weak visible light and fabrication of the resulting floating photocatalytic spheres. Sci. Rep. 9, 1–11. https://doi.org/10.1038/s41598-019-50457-w.
Wang, T., Yang, Y., Deng, Q., Zhang, X., Xiong, L., Tang, Z., Li, P., Yin, N., Sun, A., Chen, D., Shen, J., 2021a. In-situ construction of 3D marigold-like CoAl-LDH/Ti3C2 heterosystem collaborating with 2D/2D interface for efficient photodegradation of multiple antibiotics. Appl. Surf. Sci. 569, 151084 https://doi.org/10.1016/j.apsusc.2021.151084.
Wang, Y.L., Zhang, S., Zhao, Y.F., Bedia, J., Rodriguez, J.J., Belver, C., 2021b. UiO-66-based metal organic frameworks for the photodegradation of acetaminophen under simulated solar irradiation. J. Environ. Chem. Eng. 9, 106087 https://doi.org/10.1016/j.jece.2021.106087.
Wang, Y.L., Peñas-Garzón, M., Rodriguez, J.J., Bedia, J., Belver, C., 2022. Enhanced photodegradation of acetaminophen over Sr@TiO2/UiO-66-NH2 heterostructures under solar light irradiation. Chem. Eng. J. 446, 137229 https://doi.org/10.1016/j.cej.2022.137229.
Wei, Q., Xiong, S., Li, W., Jin, C., Chen, Y., Hou, L., Wu, Z., Pan, Z., He, Q., Wang, Y., Tang, D., 2021. Double Z-scheme system of α-SnWO4/UiO-66(NH2)/g-C3N4 ternary heterojunction with enhanced photocatalytic performance for ibuprofen degradation and H2 evolution. J. Alloys Compd. 885, 160984 https://doi.org/10.1016/j.jallcom.2021.160984.
Xiang, Y., Wu, H., Li, L., Ren, M., Qie, H., Lin, A., 2021. A review of distribution and risk of pharmaceuticals and personal care products in the aquatic environment in China. Ecotoxicol. Environ. Saf. 213 https://doi.org/10.1016/j.ecoenv.2021.112044.
Xu, C., Ravi Anusuyadevi, P., Aymonier, C., Luque, R., Marre, S., 2019. Nanostructured materials for photocatalysis. Chem. Soc. Rev. 48, 3868–3902. https://doi.org/10.1039/c9cs00102f.
Yang, L., Zheng, W., Zhang, P., Chen, J., Zhang, W., Tian, W.B., Sun, Z.M., 2019. Freestanding nitrogen-doped d-Ti3C2/reduced graphene oxide hybrid films for high performance supercapacitors. Electrochim. Acta 300, 349–356. https://doi.org/10.1016/j.electacta.2019.01.122.
Zhang, Z., Chen, G., Xu, K., 2013. Photoluminescence of colloids of pristine ZnAl layered double hydroxides. Ind. Eng. Chem. Res. 52, 11045–11049. https://doi.org/10.1021/ie4012326.
Zhao, Y., Wang, C.J., Gao, W., Li, B., Wang, Q., Zheng, L., Wei, M., Evans, D.G., Duan, X., O'Hare, D., 2013. Synthesis and antimicrobial activity of ZnTi-layered double hydroxide nanosheets. J. Mater. Chem. B. 1, 5988–5994. https://doi.org/10.1039/c3tb21059f.
Zhao, Y., Li, B., Wang, Q., Gao, W., Wang, C.J., Wei, M., Evans, D.G., Duan, X., O'Hare, D., 2014. NiTi-Layered double hydroxides nanosheets as efficient photocatalysts for oxygen evolution from water using visible light. Chem. Sci. 5, 951–958. https://doi.org/10.1039/c3sc52546e.
Zhao, C., Wei, Z., Zhang, J., He, P., Huang, X., Duan, X., Jia, D., Zhou, Y., 2022. Ultrafine SnO_2 nanoparticles on delaminated MXene nanosheets as an anode for lithium-ion batteries. J. Alloys Compd. 907, 164428 https://doi.org/10.1016/j.jallcom.2022.164428.
Zheng, G., Wu, C., Wang, J., Mo, S., Zou, Z., Zou, B., Long, F., 2019. Space-confined effect one-pot synthesis of γ-AlO(OH)/MgAl-LDH heterostructures with excellent adsorption performance. Nanoscale Res. Lett. 14, 281. https://doi.org/10.1186/s11671-019-3112-x.
Zhou, H., Wu, F., Fang, L., Hu, J., Luo, H., Guan, T., Hu, B.S., Zhou, M., 2020. Layered NiFe-LDH/MXene nanocomposite electrode for high-performance supercapacitor. Int. J. Hydrogen Energy 45, 13080–13089. https://doi.org/10.1016/j.ijhydene.2020.03.001.
Zhu, Y., Laipan, M., Zhu, R., Xu, T., Liu, J., Zhu, J., Xi, Y., Zhu, G., He, H., 2017. Enhanced photocatalytic activity of Zn/Ti-LDH via hybridizing with C60. Mol. Catal. 427, 54–61. https://doi.org/10.1016/j.molcata.2016.11.031.
Zhu, Y., Zhu, R., Zhu, G., Wang, M., Chen, Y., Zhu, J., Xi, Y., He, H., 2018. Plasmonic Ag coated Zn/Ti-LDH with excellent photocatalytic activity. Appl. Surf. Sci. 433, 458–467. https://doi.org/10.1016/j.apsusc.2017.09.236.
Zou, J., Wang, Z., Guo, W., Guo, B., Yu, Y., Wu, L., 2020. Photocatalytic selective oxidation of benzyl alcohol over ZnTi-LDH: the effect of surface OH groups. Appl. Catal. B Environ. 260, 118185 https://doi.org/10.1016/j.apcatb.2019.118185.
Żur, U.G.J., Piński, A., Marchlewicz, A., Hupert-Kocurek, K., Wojcieszyńska, D., 2011. Organic micropollutants paracetamol and ibuprofen—toxicity, biodegradation, and genetic background of their utilization by bacteria. Environ. Sci. Pollut. Res. 2284, 1–4. https://link.springer.com/journal/11356.